Tunneling microscopy of Ge(001)

J. A. Kubby, J. E. Griffith, R. S. Becker, and J. S. Vickers
AT&T Bell Laboratories, Murray Hill, New Jersey 07974-2070
(Received 17 February 1987; revised manuscript received 17 July 1987)

The closely related geometric and electronic structure of the Ge(001) surface have been investigated with the tunneling microscope. An asymmetric dimer reconstruction is observed that does not require vacancy-type defects for stabilization at room temperature. Regions of local (2×1), $c(4\times2)$, and $p(2\times2)$ symmetry are found, and the atomic positions in these regions are modeled with use of different arrangements of asymmetric buckled dimers. This model leads to a geometric and electronic surface configuration that is consistent with the tunneling-microscope images.

I. INTRODUCTION

The Ge(001) surface has been the subject of recent theoretical[1] and experimental[2-4] investigations. This surface is an interesting example of a system that possesses both a strong short-range interaction as well as an energetically weaker, longer-range ordering. The basic (2×1) reconstruction is generally accepted to entail the formation of dimers, created through pairing of nearest-neighbor surface atoms.[5] The driving force for pairing is bond formation with an interaction energy characteristic of chemical bonds, on the order of several electron volts. Associated with the dimer bond are two surface states roughly corresponding to the bonding and antibonding orbitals of the free diatomic molecule.

Symmetrical dimerization results in an odd number of unpaired electrons per surface atom, forming a half-filled band corresponding to a metallic surface. Such a system can spontaneously reduce its symmetry in a Jahn-Teller-type distortion. This distortion lowers the energy of the states in the occupied half of the band, thereby energetically stabilizing the surface and, at the same time, introducing a gap between the occupied and unoccupied states. Indeed, a metal-insulator transition has been observed on this surface using high-resolution angle-resolved photoemission,[2,6,7] and has been treated theoretically in terms of a structural order-disorder phase transition[8] of asymmetric dimers. Chadi[9] introduced a symmetry reducing distortion in a model of the Si(001) surface by using asymmetrical rather than symmetrical dimers. In this empirical tight-binding total-energy calculation, the optimal (2×2) and (4×2) surface reconstructions correspond to different arrangements of buckled asymmetric dimers with partially ionic bonds between dimer atoms. This model is also supported by Yin and Cohen[10] and Ihm[11] *et al.* using self-consistent pseudopotential calculations. According to the buckling model, half of the surface atoms recede towards the bulk crystal; the remaining half relax outward. In addition to buckling, where the two atoms have different perpendicular displacements, the dimer can be asymmetric in that the atoms have different parallel displacements. Rehybridization of the atomic orbitals caused by these geometrical changes may lead to charge transfer from the receding atoms to the outwardly displaced atoms,[9-12] although this is disputed.

Ordered arrangements of asymmetric dimers generate various higher-order surface reconstructions [e.g., $p(2\times2)$, $c(4\times2)$]. As the dimers are spatially separated, the interactions that drive this longer-range ordering are energetically weaker (~0.1 eV) than the driving force of bond formation (~1.0 eV) that leads to dimer formation. Accordingly, the amount of higher-order reconstruction is expected to depend sensitively on minor differences in surface preparation.

In this work we study the Ge(001) surface "topographically" and electronically with the tunneling microscope. We have obtained constant-current tunneling images that are consistent with the formation of dimers by pairing of adjacent rows of surface atoms along the $\langle 1\bar{1}0\rangle$ crystallographic directions. These images have low concentrations of missing dimer type point defects, deemphasizing the importance of π-bonded defects[13] for the Ge(001) surface reconstruction. Terraces formed from the primary (2×1) surface reconstruction were found to be separated by steps of 1.4 Å height, with the orientation of the reconstruction rotating through 90° at each monatomic step. In higher resolution images we observed domains of local $p(2\times2)$ and $c(4\times2)$ symmetry. Similar higher-order reconstructions have been recently reported in tunneling microscope studies of the Si(001) surface,[14] however this surface was found to contain a high concentration of missing dimer defects[13] that may be necessary to stabilize the buckling of dimers at room temperature.

Spectroscopic information obtained from the *I-V* characteristics of the tunnel junction at constant vacuum gap show spectral features in agreement with other surface sensitive techniques and with recent theoretical calculations[1,15] for the layer density of states (LDOS) at Γ ($\mathbf{k}_{\parallel}=0$) for filled initial states below E_F.

Comparison of images tunneling into empty sample states and tunneling out of filled sample states, collected simultaneously on either side of the surface band gap, shows that the tunneling microscope maps densities of states that are consistent with the asymmetrical buckled dimer model of this surface.[1,9-11,15]

II. EXPERIMENTAL PROCEDURES

The tunneling microscopes used in this study are similar to that described by Binnig *et al.*[16] The tunneling microscope consists of a piezoelectric tripod whose legs form an orthogonal coordinate system on which a polycrystalline tungsten probe tip is mounted. Application of 0 to 1000 V to the metallic plates evaporated on the piezoelectric legs allows the tip to be accurately positioned anywhere within a 1-μm cube. The lateral motion of the tripod was calibrated from tunneling images of the Si(111)-(7×7) reconstruction where the distances are well known. The vertical motion was calibrated by looking at small steps on the Si(111) and Ge(001) surfaces for one of the microscopes, and by electron interferometry[17] for the other microscope.

The microscope is mounted on a piezoelectric plate that is kinematically supported and capacitively clampable so that it may step the tripod-probe-tip structure in intervals of 1000 Å to 1 μm over millimeter ranges. Monitoring the field emission current between the tip and sample during the final approach allows the probe tip to be brought to within a few angstroms of the sample surface without "touching" the region to be scanned.

The tunneling probability varies both with geometric and electronic changes in the gap between the tip and sample. The particular electronic states contributing to the tunneling current can be selected to some extent by varying the magnitude and sign of the applied bias between probe tip and sample. In the limit of an applied bias V that is much less than the work function Φ, the tunneling image has been shown to represent the changing absolute position as the tip follows contours of the surface local density of states at the Fermi level (E_F) at the center of curvature of a locally spherical tip.[18] The intermediate voltage range where $V<\Phi$ has been discussed by Simmons.[19]

In the constant current mode,[16] an integrating feedback loop positions the tip with the Z piezoelectric transducer so as to maintain constant tunneling current, of magnitude 0.1 to 1 nA, between the tip and sample. As the tip is scanned laterally across the surface, the Z piezo length is corrected by the feedback loop to maintain constant tunneling current. Linear scan rates vary from 50 to 200 Å/sec; with data acquired on 1 Å boundaries, an area of 100×100 Å^2 is covered in a few minutes.

The current difference mode has been described by Hamers, Tromp, and Demuth.[30] Here the feedback control circuit used to maintain constant tunnel current is gated for short intervals during a raster scan by placing a track-and-hold circuit in the feedback loop. When the feedback loop is active, a constant voltage is applied between probe tip and sample; when inactive, the position of the tip is held stationary and the current difference between selectable pairs of bias voltages is measured. Repetition of this sequence during a raster scan allows the current-difference characteristics of each point along the raster scan to be determined simultaneously with the constant-current image.

The junction I-V characteristics are obtained with the tip held stationary over the sample surface at constant tip-sample separation. The constant gap spacing is obtained by gating the feedback loop while it is stabilizing the microscope at a demanded bias and current, then rapidly measuring the instantaneous current on a time scale too rapid for the tunneling tip to drift while the feedback loop is gated. This procedure is repeated 200 times for signal averaging. The I-V measurement is performed at various values of tip-sample separation to achieve a large dynamic range in the tunneling current, and to look for dispersion with respect to $k_\parallel$.

The measurements were carried out in two different UHV microscopes (base pressure 1×10^{-10} Torr), with facilities for *in situ* ion sputtering and direct current heating. One UHV system was equipped with a low-energy electron diffraction (LEED) apparatus for sample characterization. The samples were 1-Ω cm p-type and 0.2-Ω cm n-type Ge(001) wafers. These samples were sputter cleaned with a dose of 100 (Ar^+ or Ne^+, 1 keV) ions per surface atom. After sputtering, the samples were annealed at 800–850 °C for 1 to 20 minutes and subsequently cooled at 1 °C/sec. After this treatment a sharp two-domain (2×1) LEED pattern was observed. There was no evidence of quarter order spots or streaks that would be indicative of $c(4\times2)$ domains extending over the LEED coherence length, although some LEED investigations[6,21,22] at room temperature have found such features. These features are more commonly found on the Ge(001) surface at room temperature than on Si(001).[22] The reversible appearance of quarter order LEED spots below 230 K has been reported in an order-disorder transition on Ge(001).[2,6,7]

The probe tips were prepared by ac electrochemical polishing of 20 mil polycrystalline tungsten wire in a 1 mol NaOH solution. The probe tips were cleaned *in situ* by drawing 1–100 μA of field emission current, and in some cases the tips were sputter cleaned in order to obtain repeatable junction current-voltage characteristics.

III. RESULTS AND DISCUSSION

A. Constant-current images of the Ge(001) surface

Figure 1 shows a constant-current image of a 1Ω-cm p-type Ge(001) sample. This terrace region (~150 Å square) was acquired with a 0.1 nA demanded tunneling current at a −0.90 V bias applied between the tunnel probe tip and the sample. Under this bias condition, tunneling of electrons occurs predominantly from the Fermi surface of the probe tip into empty states above the Fermi level of the sample. The Fermi level of the clean Ge(001) surface is pinned by the surface states and the surface is expected to be strongly p type irrespective of bulk resistivity[23–26] as will be discussed below. In Fig. 1 the rows run along the $\langle 1\bar{1}0\rangle$ crystallographic direction and are separated along the $\langle 110\rangle$ direction by $a_0\sqrt{2}$ or 8 Å, where $a_0=5.66$ Å is the bulk lattice constant of Ge. This corresponds to twice the lattice constant of the unreconstructed surface $a_0/\sqrt{2}=4$ Å. It is reasonable to assume that these rows are formed by surface dimers, although the individual dimers along the row are not resolved in this low resolution image. The total range of the gray

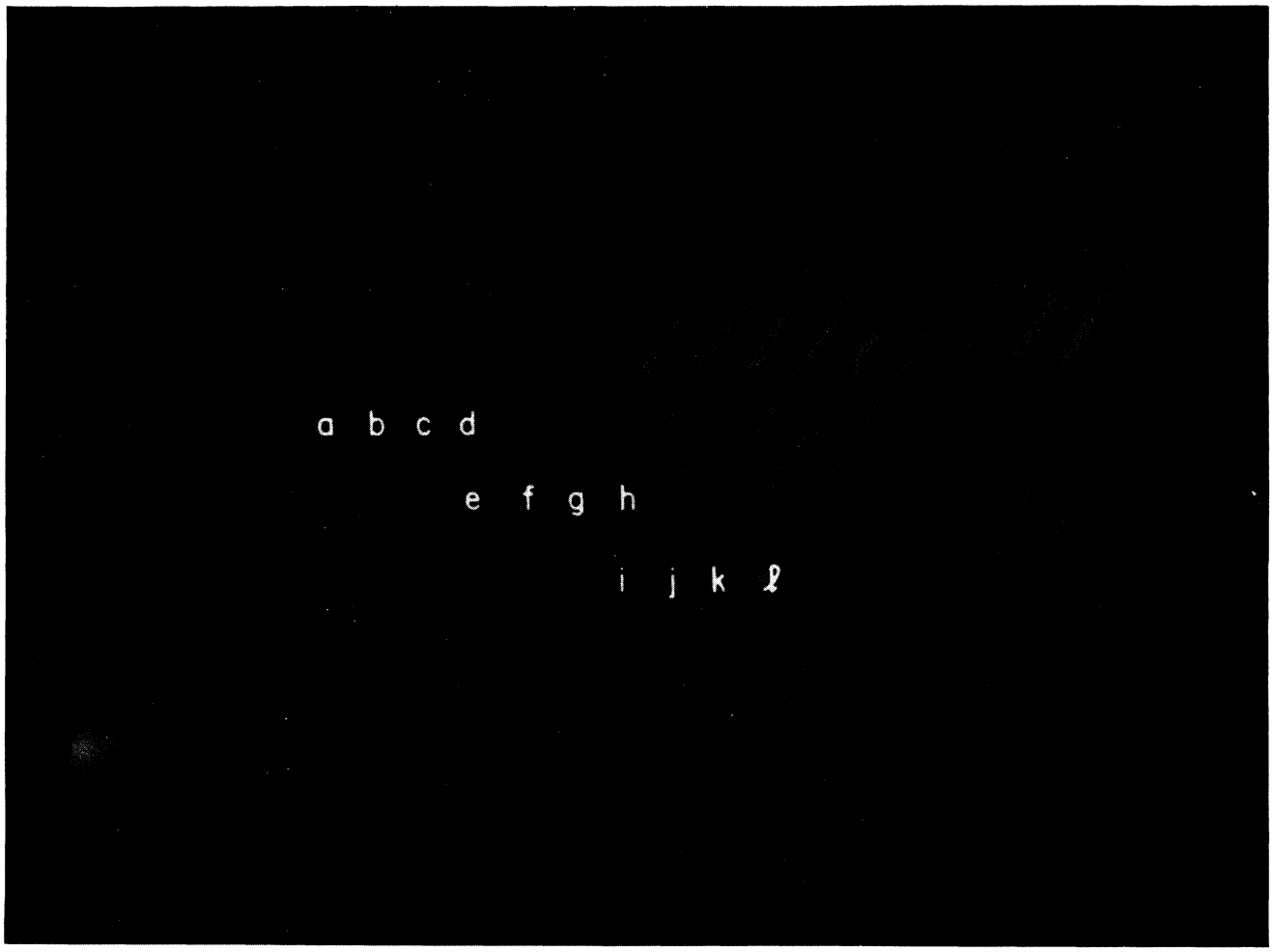

FIG. 1. Constant current tunneling microscope image of the Ge(001)-(2×1) surface. White areas are surface protrusions and black areas are depressions, with a total range of 1.5 Å. The rows run along the $\langle 1\bar{1}0\rangle$ crystallographic direction.

scale in this image is 1.5 Å with the corrugation between peaks at the top of the rows (light) and the valleys between the rows (dark) equal to 0.26 ± 0.05 Å. Under optimal operating conditions, implying maximum lateral resolution, peak to valley corrugations of 0.44 ± 0.05 Å have been measured. The defects in rows *b*, *d*, and *f* of Fig. 1 are believed to be associated with missing dimers although, without further characterization, other causes (such as adsorbate atoms) cannot be ruled out. A model for the (2×1) surface reconstruction of Si(001) given by Pandey[13] is based on missing dimer defects. This π-bonded defect model additionally incorporates defects that occur in a cross linked manner connecting different rows as seen in rows *k* and *l* in Fig. 1. It is clear, however, that the concentration of missing dimer type defects in this scan is much less than 1 in 4, the concentration predicted in the π-bonded defect model.[13]

Figure 2 shows a stepped terrace region. In this figure it can be seen that the orientation of the reconstruction rotates through 90° in terraces that are separated by monatomic steps of 1.4 Å height. This step height is close to the expected step height of $a_0/4=1.42$ Å. Because step heights and configurations on the Ge(001) surface are of interest for epitaxial growth of GaAs on a germanium substrate, we shall discuss them in more detail here.

In Fig. 2 the steps separating (001) terraces with edges in the $\langle 100\rangle$ and $\langle 110\rangle$ directions have a height of one interplanar distance $a_0/4$, although the short step to the right of rows *j*, *k*, and *l* is nearly a double step. Double steps, of height $a_0/2$, have been detected in a LEED study of vicinal Ge(001) by Olshanetsky *et al.*[27] A number of different types of steps are shown in this 150×150-Å image. In rows 5–8 of Fig. 2 the step is in the $\langle 110\rangle$ crystallographic direction with the reconstruction continuing right up to the step edge. In rows 1–4 the step is in the $\langle 100\rangle$ crystallographic direction. This step is formed from kinks (missing dimers) in the $\langle 1\bar{1}0\rangle$ direction. Similar to the $\langle 1\bar{1}0\rangle$ steps that are observed on Si(001),[14] two different configurations can occur at these steps depending on whether the atoms forming the lower step edge also

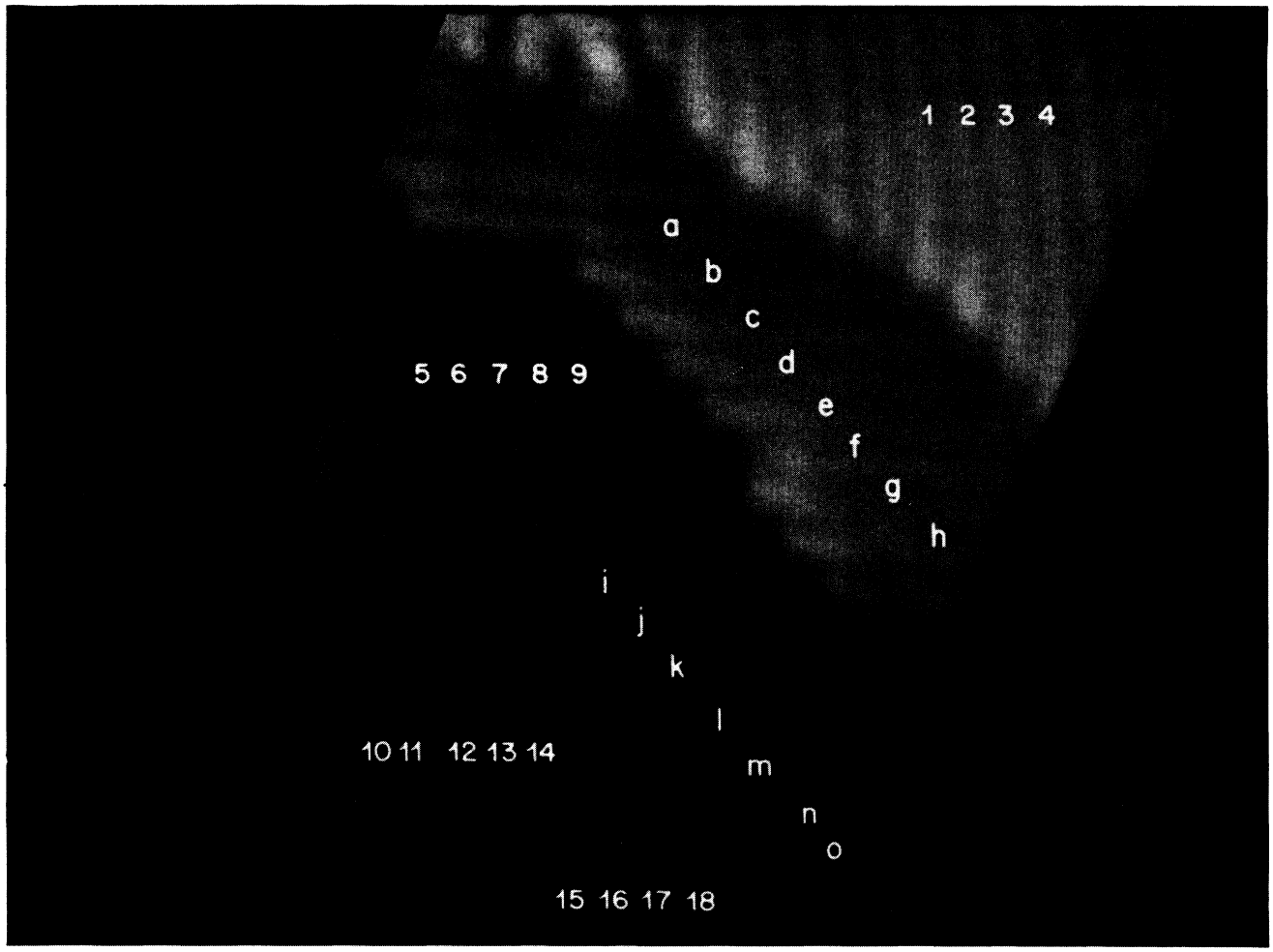

FIG. 2. Stepped terrace region. The contrast has been enhanced by light sourcing (gradient) to show all 5 terrace levels. The terraces are separated by monatomic ⟨110⟩ and ⟨100⟩ steps. The rows run along the ⟨1$\bar{1}$0⟩ direction.

participate in dimer bonding, or whether the dimer bonding starts at the next atomic row. Rows 1–4 on the upper terrace appear to terminate on valleys formed by rows $b-f$ of the lower terrace, while rows $a-e$ appear to terminate on the rows of the terrace containing rows 5–9. In the first case, the atoms forming the lower step edge participate in dimer bonding while in the second case the dimer bonding starts at the next atomic row. Steps and step related states will be considered in more detail below.

B. Electronic properties of the probe tip-sample tunnel junction

Since it has been shown in previous tunneling microscope studies of semiconductor surfaces that the electronic structure of the sample surface can dominate the geometric structure in the tunneling images,[28] no discussion of the structure of the Ge(001) surface would be complete without a discussion of the I-V characteristics of the tip-vacuum-sample gap.

As was described in Sec. II, a constant vacuum gap spacing I-V curve is obtained by gating the feedback electronics that stabilizes the microscope at a demanded bias and current, then rapidly measuring the instantaneous current on a time scale too rapid for the tunneling tip to drift while the feedback loop is gated. The resulting I-V curve, taken at stabilization biases of -2.0 and -2.5 V, and signal averaged 200 times, is shown in Fig. 3 plotted as $d\ \ln I / d\ \ln V$ against V. In this figure positive bias corresponds to tunneling from filled tip states into empty sample states, and negative bias corresponds to tunneling from filled sample states into empty tip states. The position of peaks in a plot of $d\ \ln I / d\ \ln V$ versus V are expected to show a close correspondence to the positions of resonances in the densities of states of both sample and tip.[29–31] Spectral peaks in such a plot are considered to be meaningful here only if the spectra are reproducible.

In Fig. 3 a surface state band gap of 0.9 eV width separates the filled and empty state features, although voltage drops within the sample cannot be excluded. Two

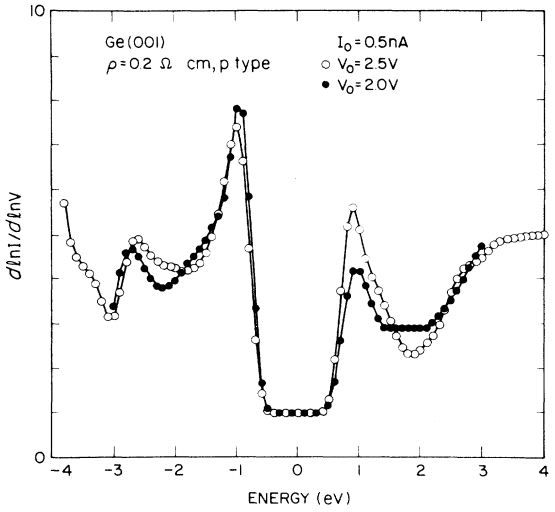

FIG. 3. The ratio of differential to total conductivity vs energy, relative to the Fermi level. Stabilization voltages of 2.0 and 2.5 V and a demanded tunneling current of 0.5 nA were used. For negative energies, tunneling occurs from filled sample states into empty tip states. For positive energies, tunneling occurs from filled tip states into empty sample states.

filled state features are found at -1.0 and -2.6 eV below the surface Fermi level and have FWHM on the order of 1 eV. An empty state peak is found at $+0.9$ eV above the Fermi level and also has a FWHM on the order of 1 eV. The features at ~ 1 eV on either side of the surface band gap were reliably reproducible, while the peak at -2.6 eV was less reproducible, and, indeed, is seen to be weaker than the features in the vicinity of zero bias. We believe the features at ± 1 eV arise mainly from the surface density of states of the germanium sample as will be discussed below. Additionally, the features at -2.6 eV may be resonant with bulk states,[32] and require a "special" configuration of the tip to reliably image.

Two different curves are shown in Fig. 3, corresponding to separations of 7.2 and 7.6 Å for stabilization voltages of -2.0 and -2.5 V, respectively, as determined by electron interferometry.[17] It can be seen that the results are almost independent of separation, showing that the exponential dependence of the transmission probability of the electron on gap separation and voltage, that appears in dI/dV, tends to cancel[29-31] in the ratio of $(dI/dV)/(I/V) = d\ln I/d\ln V$.

If the resonances in the density of states of the tip are not pronounced, the peaks in the spectra of Fig. 3 can be identified by comparison to other surface spectroscopies that are sensitive to the density of states of the sample. The peaks can also be compared to theoretical results for both surface[1,15] and bulk[32] densities of states.

The surface sensitive spectroscopic techniques can be grouped into general categories depending upon the nature of their surface sensitivity. The first group, which includes photoemission (both angle integrated and angle resolved) and inverse photoemission, owes its surface sensitivity to the elastic mean free path of an unscattered electron that limits the signal to at most a few atomic layers in the appropriate energy range of the electron. The second group, which includes field emission spectroscopy and field ionization spectroscopy, derives their surface sensitivity from a sampling of the exponential tails of the initial- and final-state wave functions of the tunneling electron. As this group of spectroscopic techniques are most closely related to the tunneling microscope, they will be considered first.

1. Tunneling spectroscopic techniques

In field emission, the final-state wave function ψ_f is known, so that the number j of electrons tunneling at given energy ϵ per unit time is sensitive to the exponential tails of the initial-state wave function ψ_i in the vacuum. In the case of field ionization, on the other hand, the initial state ψ_i is known so that $j(\epsilon)$ samples the exponential tails of the unoccupied final sample states ψ_f that are above the Fermi energy. In vacuum tunneling both the initial and final-state wave functions are unknown, so that a statement about one requires an assumption about the other. In general, an assumption is made about the tip wave function, but in the recent calculations of Lang[31,33,34] the tip is treated on an equal basis as the sample using the wave functions that arise in a self-consistent density functional calculation for a jellium surface with an adsorbed atom for both tip and sample.

The use of field emission as a probe of surface density of states below the Fermi level has been discussed by Penn and Plummer[35] and the use of field ionization for measurement of surface density of states above E_F by Penn.[36] While field-ionization spectroscopy (FIS) and field-emission spectroscopy (FES) give complementary information for the empty and filled surface states, they sample different regions of momentum space. The tunneling barrier in FES is nearly five times that in FIS so that only electrons with $k_\parallel = 0$ can contribute to the signal in FES, while electrons with a broad distribution of momenta contribute to the tunneling process in FIS.

The technique of field emission has been used by Shepherd and Peria[37] and Arthur[38] for the observation of surface state emission in the energy distribution of electrons field-emitted from (001) oriented Ge. The theory of field emission from semiconductors and the energy distribution of field-emitted electrons has been discussed by Stratton.[39] Shepherd and Peria[37] found that the field-emission energy distribution from the (001) facet of Ge exhibited a double peak. By comparing the measured distribution with theory it was shown that the lower energy peak arose from valence-band emission, while the higher peak, between 0.6 and 0.7 eV below E_F, represented emission from a band of surface states overlapping the bulk valence band. These states were localized to the center of the (001) facet and were sensitive to contamination. The peak at -1 eV in Fig. 3 also has an onset between 0.6 and 0.7 eV below E_F.

Field ionization has been used to study the empty surface states of field evaporated Ge tips. Ernst[40] and Ernst and Block[41] show the correlation between the regional brightness of field ion (FI) and field electron (FE) patterns. They interpreted the strict correspondence between FE

and FI patterns by supposing that the same surface state band discussed above takes part in field ionization as well. They felt that the high field strength (1 V/Å) in field ionization would bend the bands upward causing the surface to become p-type degenerate. The surface states just above the valence-band edge are then empty, so that electrons of the image gas atoms could then tunnel into these empty surface states. In this way, the filled (001) surface states that give rise to the regional brightness in the field-emission pattern, also have associated empty surface states that give rise to the correlated regional brightness in the field ion pattern. No kinetic energy distributions of the field-ionized noble gases were measured, so that the energy distribution of unoccupied electronic states were not determined.

If the tip used in metal-vacuum-metal tunneling exhibits nonfree-electron-like behavior, spectral features arising from the band structure of the tip could in principle be expected in a spectrum such as shown in Fig. 3. The tip used was polycrystalline tungsten, however the dimensions of the tip apex are smaller than the polycrystalline grain size so that it is essentially a single crystal; the $\langle 110 \rangle$ crystallographic direction is often found to be coincident with the tip axis in field-emission studies of polycrystalline tungsten field emitters. Field-emission and field-ionization spectroscopy have been used to show the band-structure effects exhibited by the low index faces of tungsten.

The energy distribution of electrons field-emitted from tungsten samples has been investigated by Young and Muller[42] and Swanson and Crouser.[43,44] Swanson and Crouser[43,44] found that while some of the higher index single-crystal faces exhibited free-electron-like behavior, the total energy distribution of field-emitted electrons from the $\langle 001 \rangle$ direction displayed band-structure effects. In particular, the total energy distribution for the $\langle 001 \rangle$ direction displayed a hump at 0.35 eV below the Fermi level. This filled tip state feature would give rise to a spectral peak at 0.35 eV above the Fermi level in Fig. 3, but such a feature is not apparent.

Field-ion spectroscopy has been used to study the unoccupied energy region from 0 to 4 eV above E_F on clean tungsten surfaces. Utsumi and Smith[45] identified spectral features in their field-ion energy distributions on the (001) and (011) faces of tungsten that they felt were related to surface and bulk densities of states. On the (001) face they observed spectral features at 1.3, 2.0 and 2.7 eV above E_F and related these features to peaks in theoretically determined[46] bulk (2.0 eV) and surface (1.25 and 2.7 eV) densities of states. These measurements were repeated by Hanson and Inghram[47] who only found structure at 2.0 eV above E_F. These authors also proposed alternative explanations that did not involve density of states effects. If this feature is related to the density of states, then it would give rise to a spectral peak at 2.0 eV below the Fermi level in Fig. 3, but such a feature is also not apparent. More recently the unoccupied surface states for W(001) have been investigated by inverse photoemission. At Γ, Drube *et al.*[48] observed an unoccupied surface state at 0.25 eV above the Fermi level. The angular dependence and chemisorption behavior identified it as a d_{z^2} surface state similar to the filled state observed just below E_F (Refs. 43 and 44) as discussed above. A spectral peak at $E_F+0.25$ eV is also not apparent in Fig. 3.

A further complication arises if there is structure in the I-V spectrum from adsorbates on the tip. The structure that would be expected has been discussed in the general case by Lang.[31] The specific structure that would be expected for germanium or hydrogen adsorbed on a tungsten field emitter has been discussed by Gadzuk and Plummer.[49] The role of the tip in vacuum tunneling I-V spectra can thus be dependent on the crystalline structure of the tip apex region, as well as on adsorbate atoms in this region. It is because of these possible variations in the tip structure that spectral features in $d\ \ln I / d\ \ln V$ are taken as meaningful only if the spectrum is reproducible.

2. *Other surface sensitive spectroscopic techniques*

The peaks in Fig. 3 at -1.0 and -2.6 eV can be compared to spectral peaks in photoemission data for the Ge(001) surface; however, a comparison between the two techniques must take into consideration their inherent differences. As has been discussed, the surface sensitivity of the tunneling microscope limits it to the detection of states that are confined to the surface whereas photoemission experiments may probe a few layers inside the surface, picking up bulk states as well. Although the photoelectron current in photoemission is essentially determined by the initial density of states, the intensity of a given state $|i\rangle$ is determined by the square of the matrix element $M_{fi}=\langle i|\tau|f\rangle$, where τ is the quantum-mechanical interaction of an electromagnetic field with an electron.[50] Possible selection rules that may arise in this matrix element have been discussed by Gadzuk.[51]

An angle integrated photoemission spectrum has been given by Rowe and Christman for the Ge(001) and Si(001) surfaces using photon energies in the interval $h\nu=11-21$ eV.[52] On the Ge(001) surface they found two surface sensitive features with intensities depending strongly on surface order (changed by Ar-ion bombardment) and on surface purity (changed by H, O_2, or Cl adsorption). At that time, they associated a peak at -1.3 eV with dangling bond surface states that appeared to be almost completely filled. The corresponding peak on the Si(001) surface was at -0.8 eV with respect to E_F. They also found a lower peak at -2.4 eV below E_F on Ge(001) and a corresponding peak on Si(001) at -3 eV with respect to E_F. While the spectrum of Fig. 3 also has two peaks below E_F, the peak at -2.6 eV is lower than the peak at -2.4 eV found in photoemission, and the peak at -1.0 eV in Fig. 3 is higher than the peak at -1.3 eV found in photoemission. The differences could arise from the different ranges of $k_\parallel$ sampled by these different techniques. Nonetheless, the correspondence is reasonable, especially when taking into consideration the width of the peaks (~ 1 eV FWHM) in Fig. 3.

More recently, the Ge(001) surface has been investigated with angle-resolved photoemission spectroscopy. As will be discussed below, the tunneling microscope is most sensitive to states with $\mathbf{k}_\parallel=\mathbf{0}$,[18,29,30] so that comparison with normal emission spectra for states at the Γ point of

the surface Brillouin zone are expected to be most relevant. The signal-to-background ratio for surface states relative to bulk states is also improved in angle-resolved spectroscopy. The angle-resolved photoelectron spectroscopy investigation of intrinsic surface states on the Ge reconstructed (001) surface by Nelson *et al.*[4] shows two surface states at -0.6 and -1.3 eV below the bulk valence-band maximum at the Γ point of the surface Brillouin zone. Surface sensitivity was demonstrated by the attenuation of these peaks upon oxygen exposure and a lack of dispersion (in normal emission) with photon energy in the interval of $h\nu=12-27$ eV. The intensity of these peaks varied with the incident photon energy and was interpreted in terms of atomic photoemission from states with different angular momentum quantum numbers l.[53] At low photon energies, p states have a higher photoemission cross section than s states, but the p cross section decreases with increasing photon energy much more rapidly than that for s states. Thus the photon energy dependence of the surface states at Γ indicates that they have different symmetry properties. At the lowest photon energies, the -0.6 eV peak was the most intense surface feature, while at higher photon energies the -1.3 eV peak was more intense.

A later study by Hsieh *et al.*,[3] using p-polarized light, identified peaks in their normal emission spectra at binding energies of -0.5 and -1.3 eV with respect to the valence-band maximum, but they felt that these peaks at lower photon energies ($h\nu=10-16$ eV) were in fact predominantly bulk peaks with perhaps some minor contributions from surface state transitions. At higher photon energies ($h\nu=26-45$ eV) they felt that it was very likely that these features were derived from surface state emission. These authors point out that these peaks cannot unambiguously be assigned to surface states based solely on binding energies as these energies are close to bulk related features. The peak with a measured binding energy of -1.3 eV may be associated with the $L^v_{4,5}$ or L^v_6 critical points; the theoretical[32] binding energies of $L^v_{4,5}$ and L^v_6 are -1.4 and -1.6 eV, respectively. The peak with a binding energy of -0.5 eV is also close to the theoretical binding energy (-0.3 eV) of the Γ^v_7 critical point.[32] However, Hsieh *et al.*[3] felt that this assignment was unlikely as there is no corresponding feature in the spectra that can be associated with the Γ^v_8 critical point at 0.0 eV. Thus the interpretation of these features is somewhat controversial. Hsieh *et al.*[3] did not use the contamination test used by Nelson *et al.*[4] to distinguish surface from bulk peaks, as they felt that bulk peak intensities could be changed by the suppression of surface reconstruction and surface order through surface diffraction or scattering effects, especially in the case of peaks arising from surface umklapp involving surface reconstruction.

The peak at -1 eV in Fig. 3, that extends from -1.5 to -0.5 eV, is in good overall agreement with the angle-resolved photoemission results, although the two distinct peaks at -0.5 and -1.3 eV found in photoemission experiments are not individually resolved in the tunneling spectrum. This could arise from the sensitivity of the photoemission cross section to the incident photon energy.[4] At lower photon energies, the -0.5 eV peak is the more intense feature, while at higher photon energies the -1.3-eV peak is more intense. The photoemission spectra taken with lower energy photons, that emphasize p states,[53] are in better qualitative agreement with the tunneling spectrum in Fig. 3 than photoemission spectra taken with higher energy photons, which emphasize s states.[53] As will be discussed below, the two features that are expected to contribute to peak at -1.0 eV in the tunneling spectrum have different symmetry properties, and the tunneling microscope is expected to be more sensitive to a protuberant p_z-like dangling bond state than it is to a recessed backbond state. Taking account of these symmetry considerations, the agreement between angle-resolved photoemission and the tunneling spectra is quite good.

The peak at -2.6 eV in Fig. 3, which is close in energy to the peak at -2.4 eV in the angle integrated spectra of Rowe and Christman,[52] is also close to a peak that was assigned to a direct bulk transition from the valence band along Δ_5 in the angle-resolved spectrum of Hsieh *et al.*[3] and Nelson *et al.*[4] This peak was assigned to a bulk transition because it showed a small, but nonetheless detectable, dispersion with photon energy in the interval $h\nu=10-16$ eV. Bulk states at the X point, having a large wave vector in the (001) direction, will contribute to the formation of (001) surface states and could be influential in the formation of the peak at -2.6 eV in Fig. 3. The X^v_5 critical point was determined to be near -3.0 eV in the valence-band optical densities of state by Grobman and Eastman.[32] Similar results are seen in the spectra of Hsieh *et al.*[3] and the theoretical calculations of the bulk Ge band structure.[32]

High resolution angle-resolved photoemission studies of Kevan and Stoffel[2,6,7] showed an additional feature in their normal emission spectra that is at or near the Fermi level at room temperature. This metallic surface state showed emission that was observed only over a narrow range of $k_\parallel$ near the center of the surface Brillouin zone. The state slowly disappeared as the temperature was lowered from room temperature to 77 K. This metal-insulator transition corresponded to a predicted[8] and observed[6] transition from a disordered to an ordered $c(4\times2)$ structure. In the case of the tunneling microscope I-V characteristic, by definition, $d\ln I/d\ln V=1$ at $V=0$ so that the spectrum show in Fig. 3 is not expected to show detail at E_F.

There is unfortunately much less experimental data to compare with for the empty states above E_F. In Fig. 3 a peak at 0.9 eV with a width (FWHM) on the order of 1 eV is seen. Evidence for an empty surface state can be found in the partial yield photoemission spectra for clean and adsorbate covered Ge(001) from Miller *et al.*[54] and in the joint density of states measured by ellipsometry by Meyer.[55] Meyer determined a peak at 1.7 ± 0.2 eV that could be phenomenalogically described by transitions between a band of filled surface states and a band of unfilled surface states positioned roughly symmetrically with respect to the band gap on a clean Ge(001) surface. This transition would correspond to promotion of electrons from the filled surface state at -1.0 eV to the empty surface state at $+0.9$ eV in Fig. 3. The difference in transition energy measured with the tunneling microscope (1.9

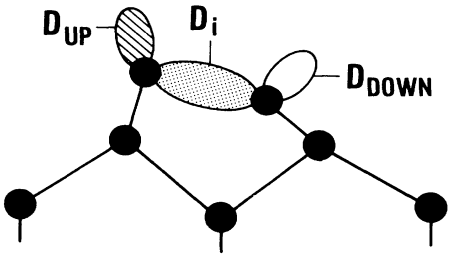

FIG. 4. The orbital character of pronounced surface features is shown schematically for the reconstructed buckled asymmetric dimer model. D_{up} and D_{down} are the filled and empty dangling bonds, respectively, and D_i is the dimer bond. The dimer antibonding orbital D_i^* as well as the backbonding B_1 and B_3 that are associated with the up and down atoms, respectively, are not shown in this figure.

eV) and that measured by ellipsometry (1.7 eV) could arise from the difference in k space emphasized by these techniques; the 1.7 eV transition in ellipsometry is a threshold energy difference that need not occur at the Γ point of the surface Brillouin zone, which is emphasized in the tunneling spectrum. Similar filled and empty state features have been determined on the related Si(001) surface by photoemission,[52,56,57] inverse photoemission,[58] reflectometry,[59] and surface photovoltage spectroscopy.[60,61]

3. Comparison to theoretical results

The peaks in $d\ln I/d\ln V$ of Fig. 3 can also be compared to the recent first-principles electronic structure theory for the Ge(001) surface given by Krüger *et al.*[1,62] and Pollman *et al.*[15] Using a local-density-functional formalism in a self-consistent scattering theoretical method, these authors determined the surface band structure for the Ge(001) surface comprised of asymmetric buckled dimers. Krüger *et al.*[1] found that the asymmetric dimer reconstruction gave rise to four salient bands that were intimately related to the surface dimer: the dimer-bond band D_i, the dangling bond band D_{up}, the dangling bond band D_{down}, and the antibonding dimer band D_i^*. The D_{up} (D_{down}) band originates from dangling bonds at the up (down) atom of the asymmetric dimer. In addition, they found back bond states that had *sp* bonding character (B_i) or mainly *s* character (S_i). The energy interval shown in Fig. 3 includes two of these backbond states; B_1 that is associated with bonding between the up atom of the dimer and the first atomic layer, and B_3 that is associated with bonding between the down atom of the dimer and the first atomic layer. A schematic representation of some of these dangling bonds is shown in Fig. 4.

The discussion of the density of states associated with a particular atom is perhaps clearest in terms of localized electronic states. A discussion of the asymmetric dimer reconstruction in terms of localized atomic levels has been given by Ihm *et al.*[11] for the related Si(001) surface. The dimer bond, D_i in Fig. 4, was described as a covalent bond [at K (-2.2 eV) on Si(001)] between p_z+p_x and p_z-p_x orbitals localized on the two atoms of the dimer (σ bonding). The corresponding antibonding combination D_i^* is not shown in Fig. 4. The filled dangling bond state D_{up} was described as developing from a bonding state of p orbitals associated with each surface atom [at J'(-0.3 eV) on Si(001)], while the unoccupied dangling-bond state of the down atom, D_{down} in Fig. 4, originated from π antibonding of the p_z states associated with the two atoms of the dimer pair [at J' (0.6 eV) on Si(001)].

The measured tunnel junction characteristics from Fig. 3 are compared to the theoretical layer density of states at the Γ point[62] (of the surface Brillouin zone) in Fig. 5. The theoretical density of states at the Γ point have been chosen for this comparison with the data as these states are expected to dominate the tunneling current. Currents arising from a state with a parallel wave vector $k_\parallel$ will decay into the vacuum with an inverse decay length $\kappa \approx (2m\bar{\phi}/\hbar^2 + k_\parallel^2)^{1/2}$, where $\bar{\phi}$ is the average barrier height.[18,29,30] For this reason, states with nonzero $k_\parallel$ have a shorter decay length and, at a given energy, states with $k_\parallel \approx 0$ will dominate the tunneling current. Only in the situation where no such states exist is it possible to observe significant tunneling to or from states with large $k_\parallel$ values.

The shaded region in the density of states in Fig. 5(a) shows the contributions of the s, p_z, and s^* orbitals to the electron density curves separately for comparison to photoemission and inverse photoemission data. Such an orbital decomposition is also of interest for comparison to tunneling spectra. As discussed by Lang,[33,34] wave functions with azimuthal quantum number $m \neq 0$ (e.g., p_{xy}

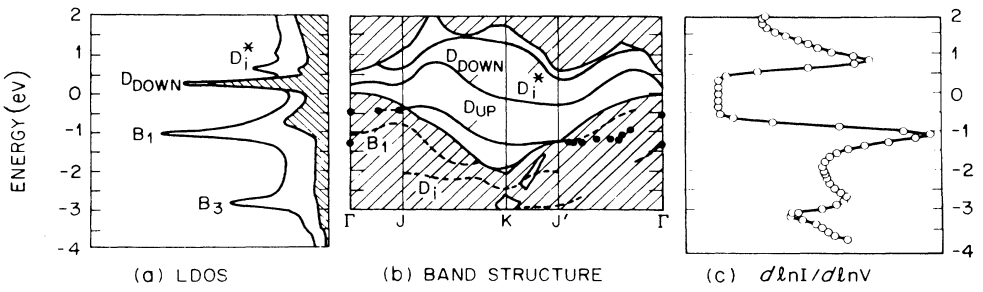

FIG. 5. Comparison of the ratio of differential to total conductivity as a function of energy (a) LDOS at Γ (from Ref. 62). The shaded region shows the s, p_z, and s^* contributions to the LDOS, separately. (b) Surface electronic band structure (from Ref. 15). The shaded region shows the bulk electronic band structure. Surface bound states are shown as solid lines and pronounced resonances are shown by dashed lines. The dots represent ARUPS data (from Ref. 4). (c) $d\ln I/d\ln V$ [from Fig. (3)].

states), have a node on the z axis, and as a consequence their main weight is towards the sample. Their contributions to the tunnel current, for lateral separations that are not too large, are smaller than those for $m=0$ (e.g., s and p_z states) that are protuberant from the surface since the current decreases exponentially with separation.

The self-consistent electronic band structure of the Ge(001) surface[15] is shown in Fig. 5(b) to indicate the dispersion of the various surface state bands. Here surface bound states are indicated by solid lines and pronounced resonances by dashed lines. The solid dots represent experimental photoemission data of Nelson *et al.*[4] All three figures have been drawn with a common energy scale on the vertical axis. The zero of the surface Fermi level in the plot of $d\ln I/d\ln V$ in Fig. 5(c) has been placed at the bulk valence-band maximum[3,23-26] in the surface band structure. The Fermi level at the surface of Ge(001) is expected to be pinned[23-26] by the filling of surface states with electrons out of the valence band[24,25] and has been measured to be within 0.1 eV of the bulk valence-band maximum.[3] This pinning of the Fermi level is confirmed by comparison of features in the photoemission spectra measured relative to the surface Fermi level,[3,52] with those measured with respect to the bulk valence-band[4,32] maximum.

Peaks occur in the theoretical LDOS at the Γ point at -2.9, -1.1, 0.2, and 0.6 eV in Fig. 5(a) that can be associated with the B_3, B_1, D_{down}, and D_i^* surface state bands, respectively. A peak associated with the D_{up} dangling-bond state has not been labeled in the LDOS of Fig. 5(a). This is because this feature becomes a broad resonance at Γ for Ge(001), giving rise to only a shoulder in the LDOS.[1,15] Although this resonance was found to be broad in energy (about 1.5 eV),[1] the surface charge density at the Γ point in the surface Brillioun zone at 0.8 eV below the valence-band maximum was found by Pollmann *et al.*[15] to have the dangling-bond character of a surface state, e.g., D_{up}. Peaks in the experimentally determined $d\ln I/d\ln V$ curves occur at -2.6, -1.0, and $+0.9$ eV as seen in Fig. 5(c). These peaks are rather broad in energy (FWHM ≈ 1 eV). The peak at -2.6 eV is close in energy to the B_3 backbond peak in Fig. 5(a) that is associated with the down atom of the dimer pair. Nonetheless, this peak is weaker than the other spectral peaks in Fig. 5(c), and may be resonant with bulk states as was described above in the discussion of photoemission spectra. As this state is a p_{xy}-like backbonding state, it is not expected to be a predominant feature in either tunneling spectra or photoemission spectra (using p-polarized light at 60° from the sample normal)[3] as both of these techniques emphasize p_z contributions relative to p_x,p_y contributions. Calculations are presently underway[62] to determine the contribution of state density that is associated with the D_i band in Fig. 5(b) to the LDOS in Fig. 5(a) around -2.6 eV for points just away from Γ in the surface Brillouin zone. The peak at -1.0 eV is intermediate in energy between the shoulder in the LDOS at -0.8 eV that is associated with the D_{up} dangling bond, and the B_1 peak at -1.1 eV that is associated with the backbond of the up atom of the dimer pair. These two features are of different symmetry types; the D_{up} states being formed from π bonding of p_z states and the B_1 state coming from p_{xy}-like backbonding states. The tunnel current could be sensitive to these different symmetries, as was discussed above in the comparison to angle-resolved photoemission spectra. Indeed, Pollmann *et al.*[15] compare the surface LDOS and surface-plane averaged charge densities $\bar{\rho}(E,z)$ at $k_{\parallel}=0$ as a function of E for $z=0$ and $z=1.25$ Å, and have found that while $\bar{\rho}(E, z=0)$ is very similar to the LDOS, $\bar{\rho}(E, z=1.25\ \text{Å})$ is drastically different, having a strong D_{up} peak at -0.80 eV and no sign of the B_1 peak that dominates $\bar{\rho}(E, z=0)$ and the LDOS. They felt that the lack of the B_1 peak in $\bar{\rho}(E, z=1.25\ \text{Å})$ was due to the fact that B_1 is a backbond resonance whose charge-density lobes are directed from the surface to the subsurface layer rather than into the vacuum. With these considerations in mind, the agreement between the experimental spectrum and the theoretical LDOS for filled states below E_F is quite good.

The peak in $d\ln I/d\ln V$ at $+0.9$ eV is significantly higher than either the 0.2- or 0.6-eV peaks in the LDOS that are associated with the D_{down} and D_i^* bands, respectively. This lack of agreement in energy position across the band gap is not surprising when comparing to a theory based on the local density approximation.[15] The band gap in the local-density-functional eigenvalues (Kohn-Sham gap ϵ_g) is typically 30–50% less than the band gap observed in the optical spectrum.[63] The band gap energy has been recently addressed by Hybertsen and Louie[64] in a first-principles theory of the quasiparticle energies in semiconductors described in terms of the electron self-energy operator. Viewed as a correction to the density functional eigenvalues calculated with the local density approximation, these results show a correction dominated by a large jump at the gap. These results were only calculated for the case of band structure in solids and an unreconstructed surface,[64] so that this correction cannot rigorously be applied to the data given here, but the results suggest that the D_{down} peak could have a substantial self-energy correction.

C. Tunneling into and out of asymmetric dimers

Figures 6 and 7 show the spatial relationship between images collected simultaneously that emphasize surface state bands on either side of the gap. When the tip is biased negatively, as in Fig. 6(a), electrons tunnel from the tip into the empty states of the sample above the Fermi level. When the polarity is reversed, as in Fig. 6(c), electrons tunnel from the filled surface states below E_F. Figure 6(b) is a superposition of figures (a) and (c) showing a clear phase shift along the dimer rows in tunneling to and from the sample.

The image shown in Fig. 6(a) (cyan) is a constant current tunneling micrograph taken with a -1.0-V potential applied to the probe tip, relative to the sample, which was held at a virtual ground. In this situation tunneling can occur from the Fermi surface of the tip into all empty sample states lying between the Fermi levels of the sample and tip. From the band structure diagram in Fig. 5, tunneling into these empty sample states would be expected to emphasize features associated with the D_{down} dangling-bond surface state, although contributions from

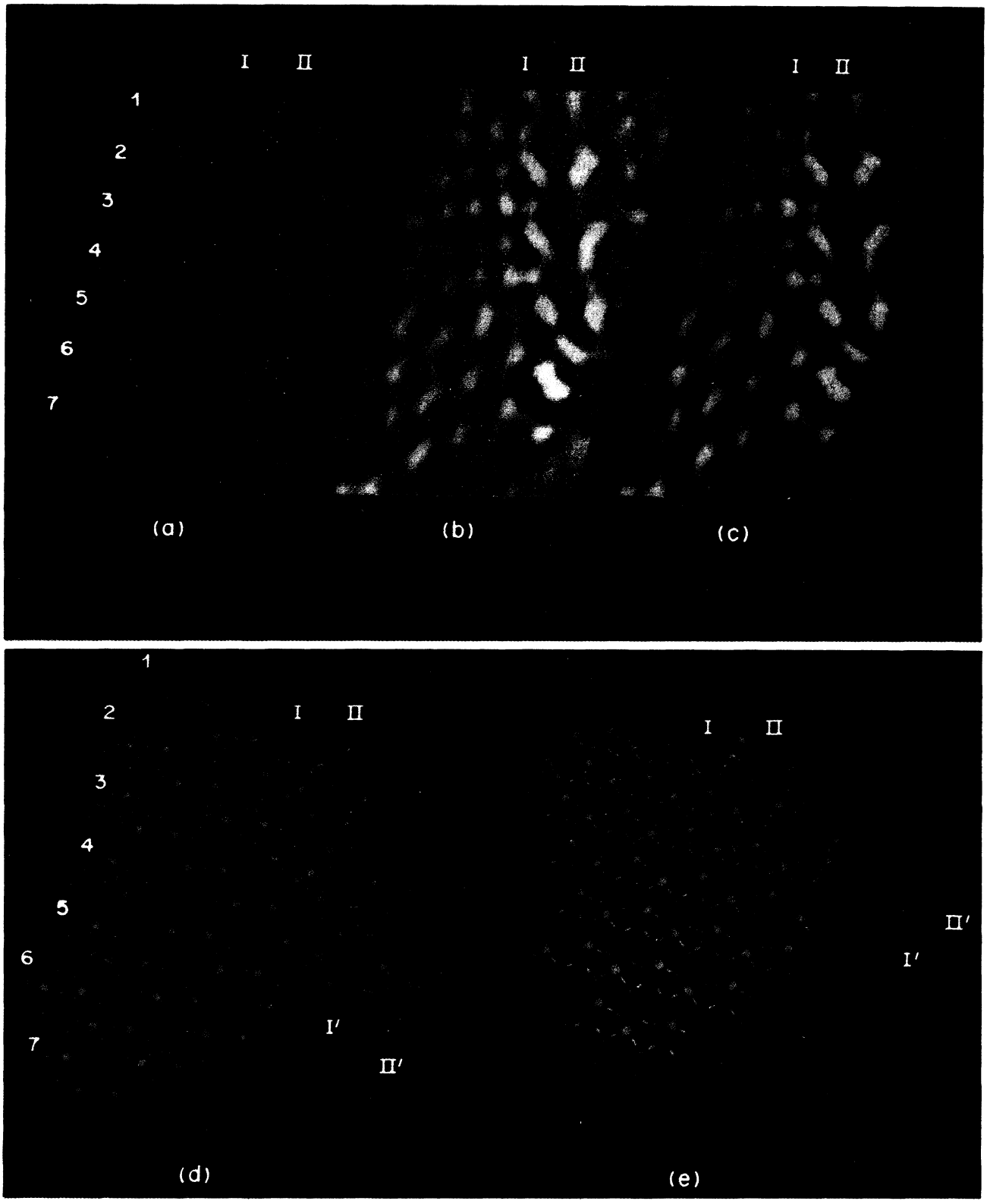

FIG. 6. (a) Constant-current image with -1 V applied to the probe tip, tunneling into empty sample states. (b) Superposition of (a) and (c) showing the phase shift between images tunneling into and out of the surface. (c) Current-difference image between $V_1 = -0.5$ and $V_2 = -1.2$ V, tunneling from filled sample states. (d) Ball and stick model of atomic positions in (a)–(c). Cyan indicates the down atom and yellow the up atom of an asymmetric buckle dimer (from Ref. 9). (e) Perspective view.

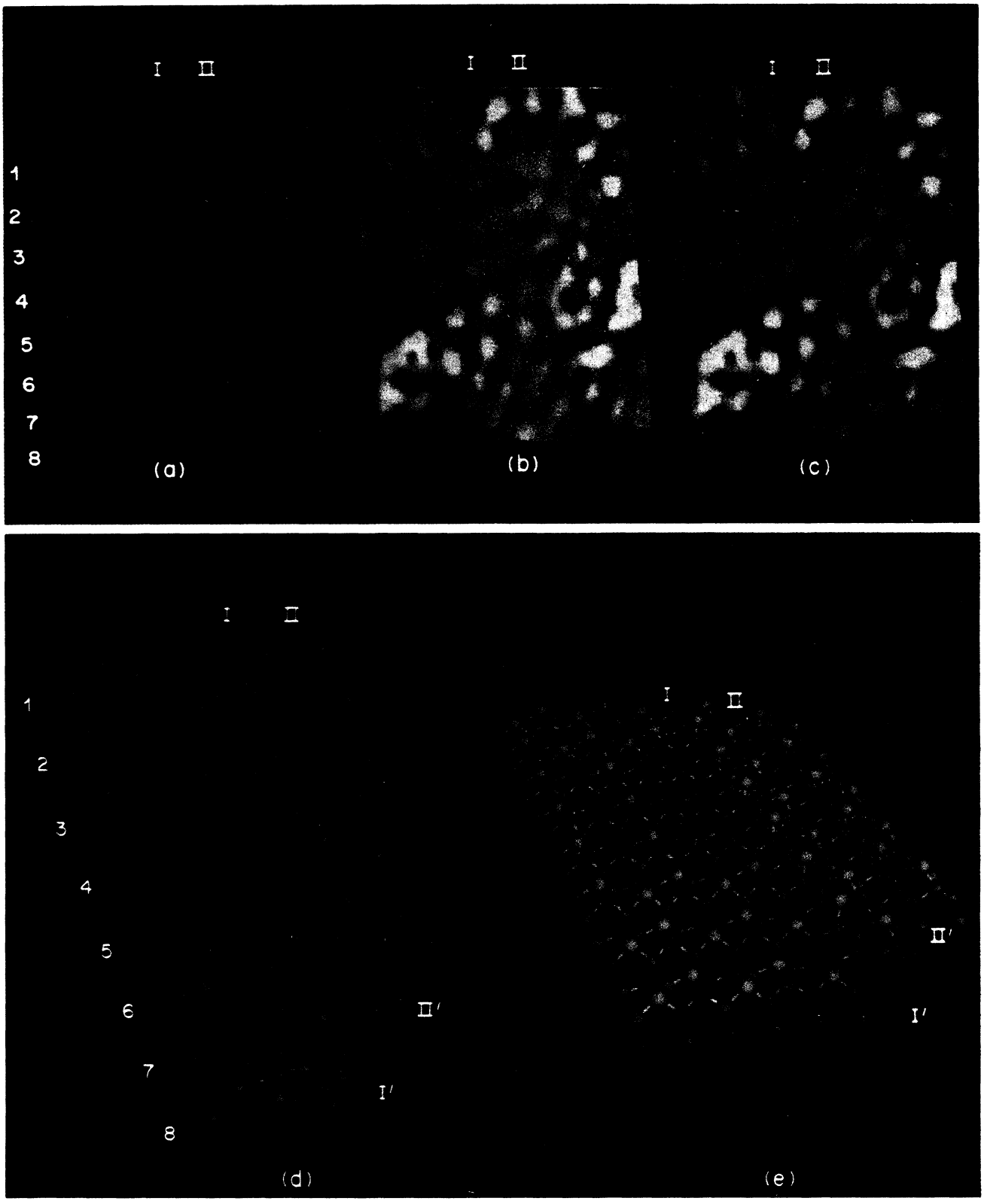

FIG. 7. Same as Fig. 6, but the step edge is now in the ⟨110⟩ crystallographic direction.

D_i^*, that are not too much higher in energy, cannot be excluded. The image in Fig. 6(c) (yellow) is a current difference image that was collected simultaneously with the tunneling image shown in Fig. 6(a). In Fig. 6(c) the current difference was taken between sample biases of -1.2 and -0.5 V, thus bracketing the peak in $d\ln I/d\ln V$ at -1.0 eV in Fig. 3. The difference image can be interpreted primarily as an image of the electronic states giving rise to this peak. From the band-structure diagram in Fig. 5(b), it would be expected that an energy window from -1.2 to -0.5 eV would bracket the filled D_{up} dangling-bond surface resonance centered at -0.8 eV at the Γ point of the surface Brillouin zone, as well as the backbond state B_1 at -1.1 eV that is associated with the D_{up} atom of the asymmetric dimer. Although there are two channels for tunneling from filled states in the energy window between -1.2 eV and -0.5 at Γ, both of these filled states are associated with D_{up} and the current-difference image can be interpreted as an image of the electronic states associated with this feature. The charge density at the Γ point associated with D_{up} at -0.8 eV is protuberant from the surface[15] and would be expected to dominate the tunneling current relative to the B_1 feature that is a backbond resonance and is recessed from the surface. Hamers *et al.*[20] have discussed the difficulty of imaging of Si-Si backbond states in the case of Si(111)-(7×7). Although it would be useful to have, it is not possible to acquire a current-difference image between $+0.5$ and $+1.2$ V, bracketing the empty state at $+1.0$ V, while stabilizing the tunneling microscope at $+1.0$ V. The feedback loop, to first order, nulls the difference in tunneling current at these two voltages that are in close proximity to the stabilization voltage. Since the tunneling process emphasizes surface states over bulk states, it is expected that the constant-current tunneling image and current-difference image collected while stabilizing the microscope at the filled state at -1.0 V would show the same spatial conformation; indeed this has been demonstrated[28] on Si(001). Figure 6(b) is a superposition of Figs. 6(a) and 6(c). This figure clearly shows a phase shift along the dimer rows that occurs when the tip bias is reversed.

Recently Stroscio *et al.*[29] have shown how the contrast in current difference images can be crucially dependent on the choice of bias voltage used for the stabilization point of the topographic image. In particular they noted a phase reversal between topographic and current-difference images that was associated with geometric changes in the tunneling gap, rather than density of state features. To check for such geometric effects we have repeated the topographic measurements, and have simultaneously collected images on either side of the surface band gap by revising the tip polarity in alternate line scans.[29] The superimposed images (cyan tunneling into empty sample states, gold tunneling out of filled simple states at ±2 eV bias) are shown in Fig. 8. The spatial conformation and phase shift between filled and empty sample states in Fig. 8 are in agreement with the images in Figs. 6 and 7, so that any geometric changes in the tunnel gap do not appear to cause a phase reversal between topographic and current difference images as was found by Stroscio *et al.*[29] on the Si(111)-2×1 surface.

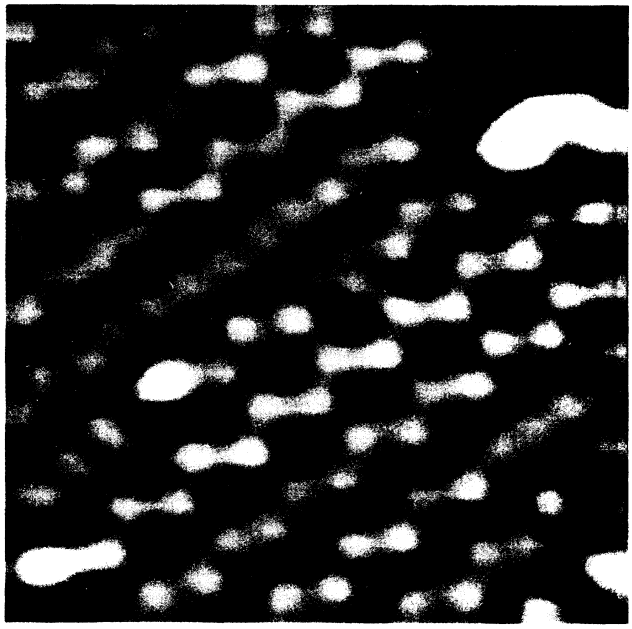

FIG. 8. Superposition of constant-current images tunneling into and out of the sample on either side of the surface band gap. The cyan image shows tunneling into empty sample states at an applied tip bias of -2 eV. The gold image shows tunneling from filled sample states at an applied tip bias of $+2$ eV. The two images were collected simultaneously by reversing the tip polarity on alternate line scans.

If the surface electronic structure is considered in a simplified model where the lower occupied surface bands around Γ are associated with states localized around the "up" atoms of the dimer pair, and the upper unoccupied surface bands around Γ are associated with the "down" atoms, then Figs. 6(a)–6(c) lead to the model structures shown in Fig. 6(d) and 6(e). Figure 6(d) is an orthographic projection of the surface structure, and 6(e) is a perspective view that emphasizes a ⟨100⟩ step between points I and I' in this figure. In Figs. 6(d) and 6(e) the atom core positions are shown, with yellow denoting an up atom and the blue denoting a down atom. The atomic displacements are based on the asymmetric dimer geometry described by Chadi[9] and Ihm *et al.*[11] for Si(001), scaled to the Ge lattice constant. We use a simple ball and stick model to indicate atomic core positions rather than the approximation of spherical atomic charge superposition, as this approximation has been shown to be substantially in error for reconstructed semiconductor surfaces.[65] A modified atomic charge superposition, that allows for different atomic charge distributions for the two dimer atoms, has recently been calculated for the Ge(001) surface.[66]

In Fig. 6(a) the rows labeled 1–7 have an apparent zigzag structure that is attributed to rows of buckled asymmetric dimers in which the direction of buckling alternates from dimer to dimer along a row. This "antiferromagnetic" ordering would be expected to lower the surface Madelung energy if a dipole moment were associated with each dimer pair. Such a dipole moment could arise

from a charge transfer from the down atom to the up atom of the dimer pair. A charge transfer of 0.36 ± 0.02 electrons results from the formation of an asymmetric dimer in Chadi's[9] model for the Si(001) surface. This surface dipole moment would result in an increase of 0.51 eV in the work function of the ionic surface relative to that of the covalently bonded (symmetric dimer) surface if screening and substrate polarization effects are ignored.[9] Experimental evidence for this extra dipole contribution to the work function of Si(001) is given in the surface photovoltage spectroscopic measurements of Mönch *et al.*[60] By using arguments based on chemical-bond theory, Pauling and Herman[32] concluded that the (001) surface of Si involved asymmetrical pairs of a tricovalent $Si^-(s^2p^3)$ atom and a tricovalent $Si^+(sp^2)$ atom, with the electric charge on Si^- and Si^+ somewhat reduced by the partial ionic character of the bonds formed by these atoms and by some resonance of the unshared electron pair from Si^- to Si^+. Evidence for a small amount of charge transfer, from the down atom to the up atom in a tilted dimer, was also found in a helium diffraction experiment to determine the surface structure of Ge(001).[65] The question of charge transfer has also been considered by Schluter[67] for the Si(001) surface. Schluter[67] points out that Chadi's empirical tight binding (ETB) calculations were done without an explicit term in the expirical Hamiltonian that would account for silicon's resistance against charge transfer (the intra-atomic Coulomb repulsion U). The *post hoc* estimate for $U\approx0.3$ eV was felt to be small.

In rows 1–3 of Fig. 6(a), correlations between the phase of buckling between the rows gives rise to local $p(2\times2)$ symmetry. We have seen no evidence of local $c(2\times2)$ symmetry. In rows 3–7, the buckling is 180° out of phase giving rise to local $c(4\times2)$ symmetry. The same local symmetry is found in the current-difference image of Fig. 6(c). Here the lozenge shapes seen in rows 4–7 are interpreted as a convolution of contributions from sources on neighboring dimer rows. The filled state maxima in Fig. 6(c) have a surface concentration of $3.12\times10^{14}/cm^2$, or normalized to the surface atom concentration of $2/a_0^2=6.24\times10^{14}/cm^2$, a factor of 1 in 2. This surface concentration is also consistent with a filled surface state associated with the up atom of an asymmetric dimer, that also occurs in a surface concentration of 1 out of every 2 surface atoms.

An interesting asymmetry is seen in rows 3–5 of Fig. (7). In Fig. 7(a), a constant current micrograph tunneling into empty sample states, these rows exhibit little or no "wiggling" amplitude associated with the alternation of buckled asymmetric dimers. Nonetheless, an asymmetry in the charge distribution can be seen from the superposition of the filled and empty state tunneling images in Fig. 7(b). The yellow, emphasizing the filled sample states shown in the current difference image of Fig. 7(c), is weighted towards the top of rows 3–5 in Fig. 7(b). Thus even in the case of local (2×1) symmetry, the dimers can exhibit asymmetric behavior. This local (2×1) domain is a boundary region between the local $c(4\times2)$ symmetry of rows (1,2) and (6,7). Rows 2 and 7 show the behavior at phase boundaries between regions of local symmetry, as well as varying degrees of asymmetry for the tilting of the dimers.

The electronic structure of the Si(001) surface has been recently investigated by Hamers *et al.*[28] with the tunneling microscope. These investigators found one filled and one empty state in the energy interval of -2 to $+2$ eV with respect to the surface Fermi level, and identified these states with atomic features of a dimer model. They concluded that tunneling from filled sample states occurred exclusively though the Si-Si dimer bond, while tunneling into the sample occurs through the empty dangling bonds for symmetric looking dimers. Hamers *et al.*[28] were unable to ascertain with their tunneling images whether the symmetric-looking dimers were truly symmetric or whether they were only sensitive to the time-average position of dimers that were rapidly switching between the two buckling directions. These authors point out that the ion scattering studies of Tromp *et al.*[68] find best agreement for buckled dimer models. The buckled dimer model was also supported by the helium diffraction experiment of Cardillo and Becker[69] for the reconstructed Si(001) surface, and by Lambert *et al.*[66] for the Ge(001) surface.

In tunneling microscope images of Si(001), Tromp *et al.*[14] and Hamers *et al.*[14] also observed buckled dimers, but only close to point defects. Based on the location of the buckled dimers near defects, they argued that the buckled dimers observed with the tunneling microscope at room temperature were stabilized by defects. When the dimers were buckled, they found different electronic structures on each of the two atoms. The atom that appeared highest at negative sample bias gave rise to the least tunneling current at positive sample bias and vice versa. Hamers *et al.*[28] gave this as evidence for a transfer of charge from the lower atom to the upper atom upon buckling, since the single filled state is localized on the upper atom while the single empty state is localized on the lower atom.

D. Step related states

Two of the different step configurations that were shown in the stepped terrace of Fig. 2 occur separately in Figs. 6 and 7. In Fig. 6(a) the step labeled I is in the $\langle 100\rangle$ crystallographic direction. This step is formed from kinks (missing dimers) in the $\langle 1\bar{1}0\rangle$ direction. This step appears between point I and I′ of the models in Figs. 6(d) and 6(e). Another $\langle 100\rangle$ step is shown between points II and II′. The atomic positions in this model have been indicated in such a way that the atoms forming the lower step edge do not participate in dimer bonding. These atoms are colored yellow as they also have dangling bonds forming a (111) minifacet at the step edge. These two dangling tetrahedral bonds show up very predominately in the current-difference image of Fig. 6(c) along lines I and II, and contribute to current-difference images that bracket the surface band gap.

Figure 7 has a step in the $\langle 110\rangle$ direction that has been labeled I in each of the images. It can be seen that the dimer reconstruction extends right up to the step edge here.

In Fig. 7(b) and the models in Figs. 7(d) and 7(e), the yellow that has been associated with the up atom of the dimer is in line with the rows in the terrace below. The cyan that runs along the upper step edge is in line with the valleys formed between the dimer rows on the lower terrace. This observation is in agreement with the steps that were observed on the Si(001) surface.[14] Here the up atoms in the upper plane step edge were always aligned with the center of the dimer in the lower plane while the down atoms were aligned with the gap between dimer rows in the lower plane.

IV. CONCLUSIONS

We have found that the predominant reconstruction mechanism for the Ge(001) surface is dimerization.[5] The concentration of missing dimer point defects is much less than on the Si(001) surface,[14] and they do not appear to be necessary for either the (2×1) surface reconstruction, or for higher-order $p(2\times2)$ and $c(4\times2)$ ordering.[13] We have found no evidence for a $c(2\times2)$ ordering.

Our tunneling images and I-V spectra for filled sample states are in good qualitative and quantitative agreement with previous observations of surface state emission in the energy and emissivity distributions of electrons field-emitted from (001) oriented Ge.[35,36] We have found qualitative agreement between our tunneling images for empty sample states and the regional brightness of field ion images, where electrons of the image gas tunnel preferentially into empty surface states.[38,39] Our tunneling spectra have also been found to be free of nonfree-electron-like behavior of the tungsten probe tip.

Our tunneling spectra have been compared to other surface sensitive techniques.[2-4,52-55] The best agreement is found for techniques that emphasize the $\mathbf{k}_{\parallel}=0$ region of momentum space.[3,4] We have found that symmetry considerations can also be important.[4,53]

The peaks in $d\ln I/d\ln V$ below E_F are also in agreement with spectral features in the layer density of states at Γ in a first-principles electronic structure theory[1,15,62] for the Ge(001) surface comprised of asymmetrical buckled dimers. The agreement with other experimental techniques mentioned above, as well as with theoretical predictions, suggests that $d\ln I/d\ln V$ is related to the LDOS (Refs. 29–31) on Ge (001) and that the tunneling current is dominated by states near Γ for sufficient probe tip to sample separation.[18,29,30]

A simplified model of the atomic positions using Chadi's asymmetric dimer configuration,[9] that associates a lower occupied surface band corresponding to electronic states localized around the up atom and an empty upper band corresponding to states associated with the down atom of an asymmetric dimer, leads to a geometric and electronic surface configuration that is consistent with the tunneling microscope images.

The Ge(001) surface has been found to be comprised of asymmetric dimers at room temperature that do not require point defects for stabilization in contrast to Si(001). The asymmetric dimers are arranged in local $p(2\times2)$ and $c(4\times2)$ domains that are stable at room temperature, suggesting that the low-temperature phase transition predicted[8] and seen[2,6,7] on this surface is more complex than a simple dimer flip and may involve collective interactions.

Steps on this surface are of monatomic height, and occur in primarily two configurations. In one configuration the steps are in the $\langle 110\rangle$ direction, with the dimer pair reconstruction extending up to the step edge. In the other configuration the step is in the $\langle 100\rangle$ direction, and is comprised of kinks formed by missing dimers. This step configuration has a higher linear density of filled dangling-bond states than the $\langle 100\rangle$ steps.

ACKNOWLEDGMENTS

We would like to acknowledge helpful discussions with E. G. McRae, R. Malic, J. E. Rowe, M. Schlüter, and M. S. Hybertsen at AT&T Bell Laboratories, P. E. Wierenga of Philips Research Laboratories, Eindhoven, the Netherlands, J. Pollmann of Münster University, West Germany, and R. M. Feenstra of IBM Thomas J. Watson Laboratory.

[1] P. Krüger, A. Mazur, J. Pollmann, and G. Wolfgarten, Phys. Rev. Lett. **57**, 1468 (1986); M. Needels, M. C. Payne, and J. D. Joannopoulos, *ibid.* **58**, 1765 (1987).

[2] S. D. Kevan and N. G. Stoffel, Phys. Rev. Lett. **53**, 702 (1984).

[3] T. C. Hsieh, T. Miller, and T.-C. Chiang, Phys. Rev. B **30**, 7005 (1984).

[4] Jeffrey G. Nelson, William J. Gignac, R. Stanley Williams, Steven W. Robey, J. G. Tobin, and D. A. Shirley, Phys. Rev. B **27**, 3924 (1983); see also Jeffrey G. Nelson, William J. Gignac, R. Stanley Williams, Steven W. Robey, J. G. Tobin, and D. A. Shirley, Surf. Sci. **131**, 290 (1983).

[5] R. E. Schlier and H. E. Farnsworth, J. Chem. Phys. **30**, 917 (1959); see also J. D. Levine, Surf. Sci. **34**, 90 (1973).

[6] S. D. Kevan, Phys. Rev. B **32**, 2344 (1985). See also R. J. Culbertson, Y. Kuk, and L. C. Feldman, Surf. Sci. **167**, 127 (1986).

[7] S. Kevan and N. G. Stoffel, J. Vac. Sci. Technol. A **3**, 1497 (1985).

[8] J. Ihm, D. H. Lee, J. D. Joannopoulos, and J. J. Xiong, Phys. Rev. Lett. **51**, 1872 (1983).

[9] D. J. Chadi, Phys. Rev. Lett. **43**, 43 (1979); see also D. J. Chadi, J. Vac. Sci. Technol. **16**, 1290 (1979), and D. J. Chadi, Appl. Opt. **19**, 3971 (1980).

[10] M. T. Yin and M. L. Cohen, Phys. Rev. B **24**, 2303 (1981).

[11] J. Ihm, M. L. Cohen, and D. J. Chadi, Phys. Rev. B **21**, 4592 (1980).

[12] L. Pauling and Z. S. Herman, Phys. Rev. B **28**, 6154 (1983).

[13] K. C. Pandey, in *Proceedings of the Seventeenth International Conference on the Physics of Semiconductors, San Francisco, 1984*, edited by D. J. Chadi and W. A. Harrison (Springer-Verlag, New York, 1985), p. 55.

[14] R. M. Tromp, R. J. Hamers, and J. E. Demuth, Phys. Rev. Lett. **55**, 1303 (1985); R. J. Hamers, R. M. Tromp, and J. E. Demuth, Phys. Rev. B **34**, 5343 (1986).

[15] J. Pollman, P. Krüger, A. Mazur, and G. Wolfgarten, in

Proceedings of the Eighteenth International Conference on the Physics of Semiconductors, edited by O. Engström (World Scientific, Singapore, 1986), p. 81; see also J. Pollman, P. Krüger, and A. Mazur, J. Vac. Sci. Technol. B **5**, 945 (1987).

[16]G. Binnig, H. Rohrer, Ch. Gerber, and E. Weibel, Phys. Rev. Lett. **50**, 120 (1983).

[17]R. S. Becker, J. A. Golovchenko, and B. S. Swartzentruber, Phys. Rev. Lett. **55**, 987 (1985).

[18]J. Tersoff and D. R. Hamann, Phys. Rev. Lett. **50**, 1998 (1983); see also J. Tersoff and D. R. Hamann, Phys. Rev. B **31**, 805 (1985).

[19]John G. Simmons, J. Appl. Phys. **34**, 1793 (1963).

[20]R. J. Hamers, R. M. Tromp, and J. E. Demuth, Phys. Rev. Lett. **56**, 1972 (1986).

[21]B. Z. Olshanetsky, S. M. Repinsky, and A. A. Shklyaev, Surf. Sci. **64**, 224 (1977).

[22]F. Jona, H. D. Shih, D. W. Jepsen, and P. M. Marcus, J. Phys. C **12**, L455 (1979); see also J. C. Fernandez, W. S. Yang, H. D. Shih, F. Jona, D. W. Jepsen, and P. M. Marcus, *ibid.*, **14**, L55 (1981).

[23]W. H. Brattain and J. Bardeen, Phys. Rev. **74**, 231 (1948).

[24]P. Handler and W. M. Portnoy, Phys. Rev. **116**, 516 (1959).

[25]R. Forman, Phys. Rev. **117**, 698 (1960).

[26]Y. Margoninski, Phys. Rev. **132**, 1910 (1963).

[27]B. Z. Olshanetsky, S. M. Repinsky, and A. A. Shklyaev, Surf. Sci. **69**, 205 (1977).

[28]R. J. Hamers, R. M. Tromp, and J. E. Demuth, Surf. Sci. **181**, 3846 (1987); J. Tersoff, Phys. Rev. Lett. **57**, 440 (1986).

[29]Joseph A. Stroscio, R. M. Feenstra, and A. P. Fein, Phys. Rev. Lett. **57**, 2579 (1986). The phase reversal between topographic and current-difference images has been discussed by Joseph A. Stroscio, R. M. Feenstra, and A. P. Fein, J. Vac. Sci. Technol. A **5**, 838 (1987).

[30]R. M. Feenstra, Joseph A. Stroscio, and A. P. Fein, Surf. Sci. **181**, 295 (1987).

[31]N. D. Lang, Phys. Rev. B **34**, 5947 (1986).

[32]J. R. Chelikowsky and M. L. Cohen, Phys. Rev. B **14**, 556 (1976). See also J. C. Phillips, D. Brust, and F. Bassani, in *Proceedings of the International Conference on the Physics of Semiconductors, Exeter, 1962* (The Institute of Physics, London, 1962), p. 564. Experimental values for germanium valence-band optical densities of state were given in W. D. Grobman and D. E. Eastman, Phys. Rev. Lett. **29**, 1508 (1972).

[33]N. D. Lang, Phys. Rev. Lett. **55**, 230 (1985).

[34]N. D. Lang, Phys. Rev. Lett. **56**, 1164 (1986).

[35]David R. Penn and E. W. Plummer, Phys. Rev. B **9**, 1216 (1974).

[36]David R. Penn, Surf. Sci. **52**, 270 (1975).

[37]W. B. Shepherd and W. T. Peria, Surf. Sci. **38**, 461 (1973).

[38]J. R. Arthur, Surf. Sci. **2**, 389 (1964); J. Appl. Phys. **36**, 3221 (1965).

[39]Robert Stratton, Phys. Rev. **125**, 67 (1962); Phys. Rev. **135**, A794 (1964).

[40]Lajus Ernst, Surf. Sci. **32**, 387 (1972).

[41]L. Ernst and J. H. Block, Surf. Sci. **49**, 293 (1975).

[42]Russel D. Young and Erwin W. Müller, Phys. Rev. **113**, 115 (1959).

[43]L. W. Swanson and L. C. Crouser, Phys. Rev. Lett. **16**, 389 (1966); see also E. W. Plummer and J. W. Gadzuk, Phys. Rev. Lett. **25**, 1493 (1970).

[44]L. W. Swanson and L. C. Crouser, Phys. Rev. **163**, 622 (1967).

[45]T. Utsumi and N. V. Smith, Phys. Rev. Lett. **33**, 1294 (1974).

[46]N. Egede Christensen and B. Feuerbacher, Phys. Rev. B **10**, 2349 (1974); see also M. Posternak, H. Krakauer, A. J. Freeman, and D. D. Koeling, *ibid.*, **21**, 5601 (1980), and L. F. Mattheiss and D. R. Hamann *ibid.*, **29**, 5372 (1984).

[47]Gary R. Hanson and Mark G. Inhgram, Surf. Sci. **55**, 29 (1976); see also Gray R. Hanson and Mark G. Inghram, *ibid.*, **64**, 305 (1977)

[48]W. Drube, D. Straub, F. J. Himpsel, P. Soukiassian, C. L. Fu, and A. J. Freeman, Phys. Rev. B **34**, 8989 (1986).

[49]J. W. Gadzuk and E. W. Plummer, Rev. Mod. Phys. **45**, 487 (1973).

[50]B. Feuerbacher and B. Fitton, in *Electron Spectroscopy for Surface Analysis,* edited by H. Ibach (Springer-Verlag, Berlin, 1977), p. 151.

[51]J. Gadzuk, in *Electronic Structure and Reactivity of Metal Surfaces,* edited by E. G. Derouane and A. A. Lucas (Plenum, London, 1976).

[52]J. E. Rowe and S. B. Christman, J. Vac. Sci. Technol. **17**, 220 (1980).

[53]R. S. Williams and D. A. Shirley, J. Chem. Phys. **66**, 2378 (1977).

[54]T. Miller, E. Rosenwinkel, and T.-C. Chiang, Solid State Commun. **47**, 935 (1983).

[55]F. Meyer, Phys. Rev. B **9**, 3622 (1974).

[56]F. J. Himpsel and D. E. Eastman, J. Vac. Sci. Technol. **16**, 1297 (1979).

[57]R. I. G. Uhrberg, G. V. Hansson, J. M. Nicholls, and S. A. Flodström, Phys. Rev. B **24**, 4684 (1981).

[58]F. J. Himpsel and Th. Fauster, J. Vac. Sci. Technol. A **2**, 815 (1984).

[59]P. E. Wierenga, M. J. Sparnaay, and van Silfhout, Surf. Sci. **99**, 59 (1980).

[60]W. Möch, P. Koke, and S. Krueger, J. Vac. Sci. Technol. **19**, 313 (1981).

[61]P. Koke and W. Mönch, Solid State Commun. **36**, 1007 (1980).

[62]P. Krüger and J. Pollmann (private communication).

[63]*Theory of the Inhomogeneous Electron Gas,* edited by S. Lundquist and N. H. March (Plenum, New York, 1983), and references therein. The error in the local-density-functional eigenvalues has been explained by Shan and Schlüter as due to a so far overlooked subtlety in the density-functional theory as discussed in L. J. Shan and M. Schlüter, Phys. Rev. Lett. **51**, 1888 (1983).

[64]Mark S. Hybertsen and Steven G. Louie, Phys. Rev. Lett. **55**, 1418 (1985); see also Mark S. Hybertsen and Steven G. Louie, Phys. Rev. B **34**, 5390 (1986); and R. W. Godby, M. Schlüter, and L. J. Sham, Phys. Rev. Lett. **56**, 2415 (1986). A many-body calculation of surface states for the Ge(111)-As surface show a substantially larger gap between the empty and occupied surface states in comparison to local-density-functional calculations. See Mark S. Hybertsen and Steven G. Louie, Phys. Rev. Lett. **58**, 1551 (1987).

[65]A. Sakai, M. J. Cardillo, and D. R. Hamann, Phys. Rev. B **33**, 5774 (1986).

[66]W. R. Lambert, P. L. Trevor, M. J. Cardillo, A. Sakai, and D. R. Hamann, Phys. Rev. B **35**, 8055 (1987).

[67]M. Schlüter, in *The Chemical Physics of Solid Surfaces and Heterogeneous Catalysis* (in press).

[68]R. M. Tromp, R. G. Smeenk, and F. W. Saris, Phys. Rev. Lett. **46**, 939 (1981); see also R. M. Tromp, R. G. Smeenk, and F. W. Saris, Surf. Sci. **133**, 137 (1983).

[69]Mark J. Cardillo and G. E. Becker, Phys. Rev. Lett. **40**, 1148 (1978); see also Mark J. Cardillo and G. E. Becker, Phys. Rev. B **21**, 1497 (1980).

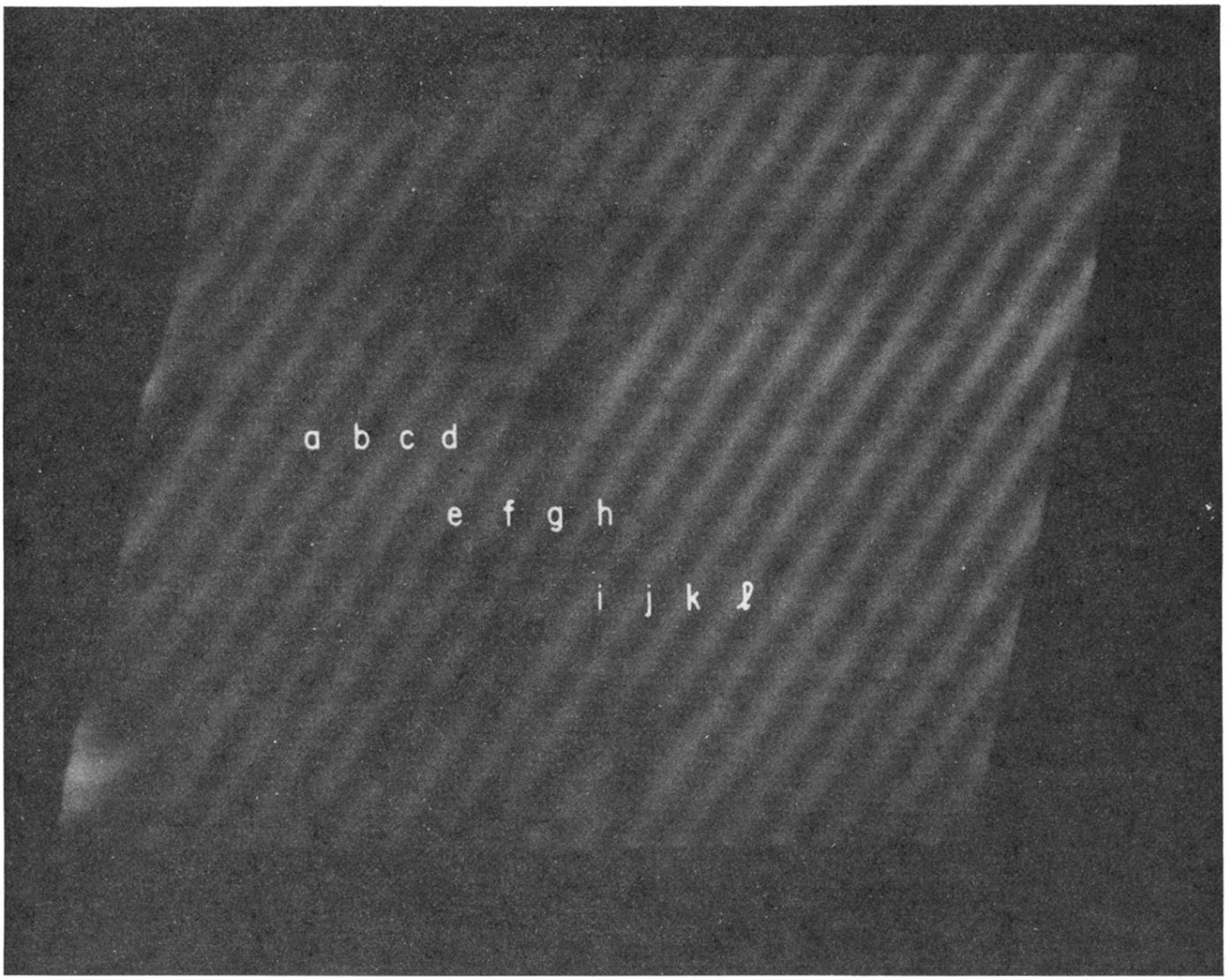

FIG. 1. Constant current tunneling microscope image of the Ge(001)-(2×1) surface. White areas are surface protrusions and black areas are depressions, with a total range of 1.5 Å. The rows run along the $\langle 1\bar{1}0 \rangle$ crystallographic direction.

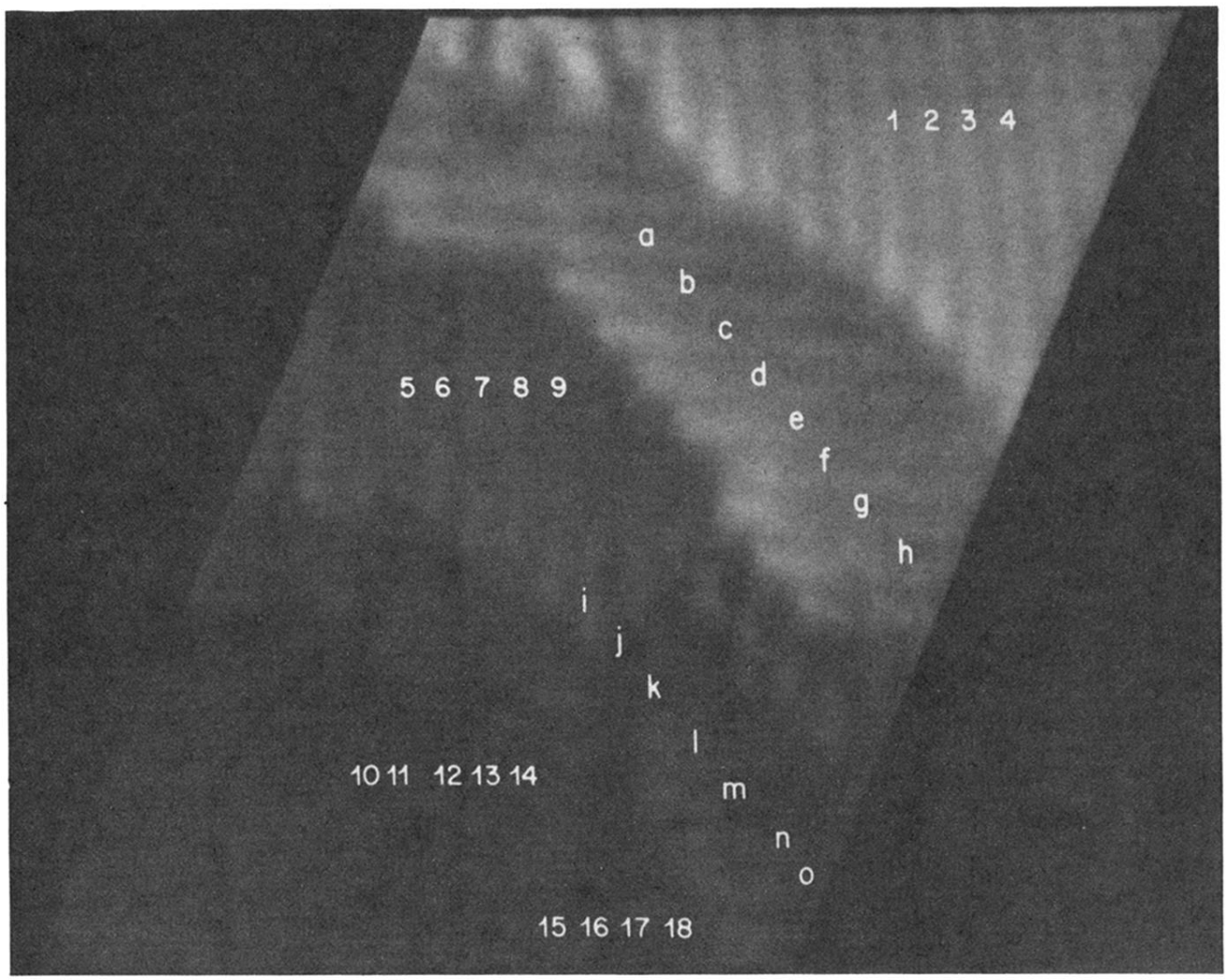

FIG. 2. Stepped terrace region. The contrast has been enhanced by light sourcing (gradient) to show all 5 terrace levels. The terraces are separated by monatomic ⟨110⟩ and ⟨100⟩ steps. The rows run along the ⟨1$\bar{1}$0⟩ direction.

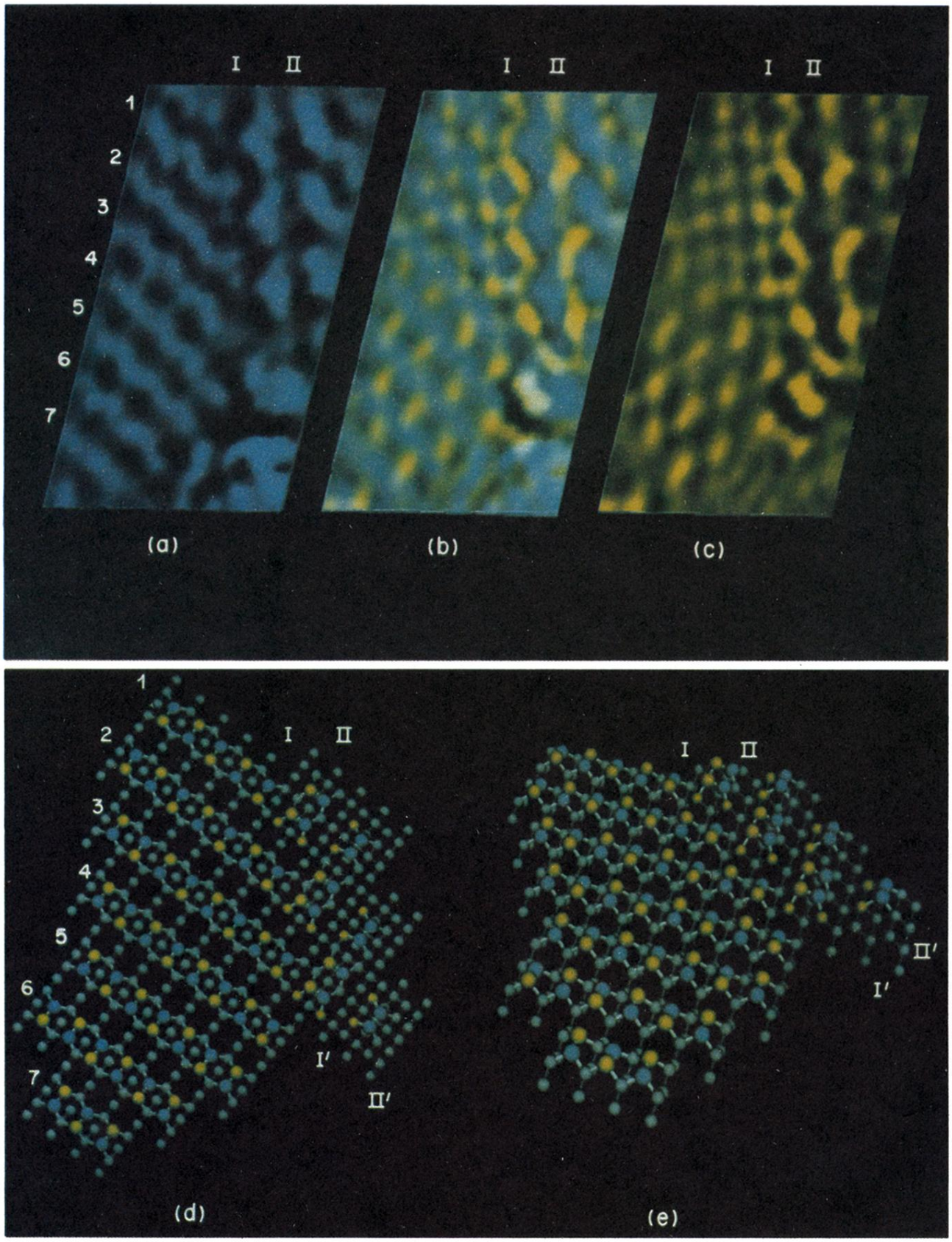

FIG. 6. (a) Constant-current image with -1 V applied to the probe tip, tunneling into empty sample states. (b) Superposition of (a) and (c) showing the phase shift between images tunneling into and out of the surface. (c) Current-difference image between $V_1 = -0.5$ and $V_2 = -1.2$ V, tunneling from filled sample states. (d) Ball and stick model of atomic positions in (a)–(c). Cyan indicates the down atom and yellow the up atom of an asymmetric buckle dimer (from Ref. 9). (e) Perspective view.

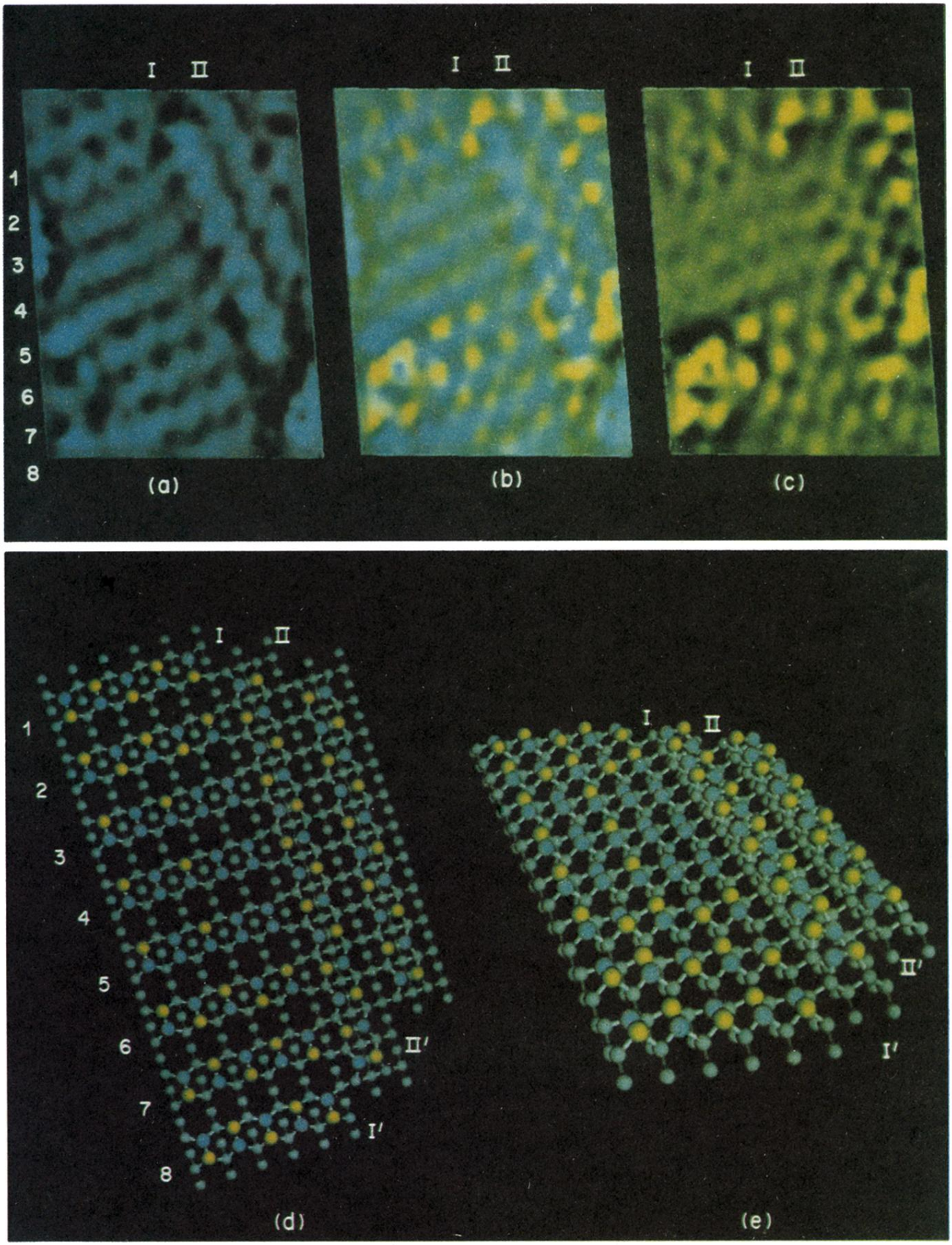

FIG. 7. Same as Fig. 6, but the step edge is now in the ⟨110⟩ crystallographic direction.

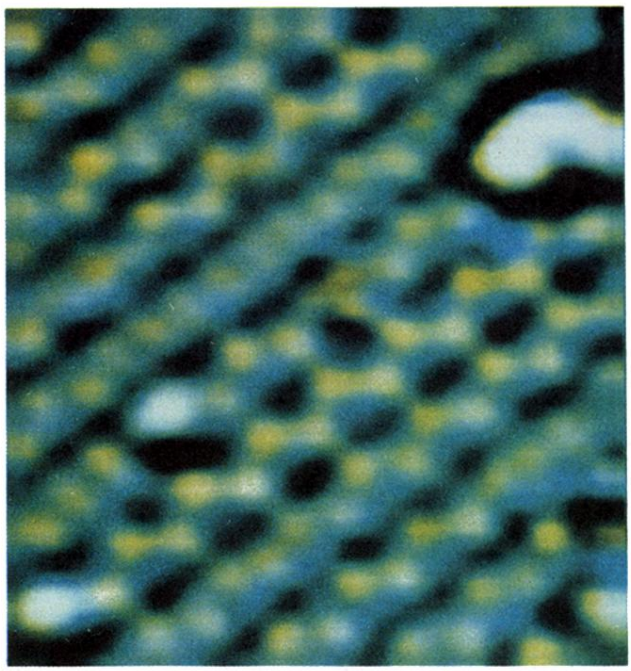

FIG. 8. Superposition of constant-current images tunneling into and out of the sample on either side of the surface band gap. The cyan image shows tunneling into empty sample states at an applied tip bias of -2 eV. The gold image shows tunneling from filled sample states at an applied tip bias of $+2$ eV. The two images were collected simultaneously by reversing the tip polarity on alternate line scans.